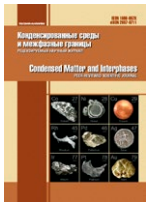

ISSN 1606-867X (Print)
ISSN 2687-0711 (Online)
Condensed Matter and Interphases
Kondensirovannye Sredy i Mezhfaznye Granitsy
https://journals.vsu.ru/kcmf/

Original articles

Research article
https://doi.org/10.17308/kcmf.2023.25/11104

The effect of the synthesis conditions on the crystal structure of palladium(II) oxide nanofilms

A. M. Samoylov[1]✉, S.S. Kopytin[1], S.A. Ivkov[1], E. A. Ratkov[1], E. A. Tutov[2]

[1]Voronezh State University,
1 Universitetskaya pl., Voronezh 394018, Russian Federation

[2]Voronezh State Technical University,
84 20 letiya Oktyabrya st., Voronezh, 394006, Russian Federation

Abstract

Nanocrystalline films of palladium(II) oxide obtained by oxidation of the initial metallic Pd layers with a thickness of 35 nm on Si (100) substrates in atmospheric air were studied using XRD analysis, TEM, and RHEED.

PdO/SiO_2/Si (100) heterostructures were synthesised in two stages. First, we obtained finely dispersed layers of metallic Pd on SiO_2/Si (100) substrates with an ~ 300 nm SiO_2 buffer layer using thermal sublimation in a high vacuum. The Pd layers were then oxidised in the temperature range T_{ox} = 620 – 1100 K in atmospheric air (with the partial pressure of oxygen of about 21 kPa). The study determined that the deformation of the tetragonal crystal structure of homogeneous nanocrystalline PdO films is explained by an increase in the values of lattice parameters with the oxidation temperature. The deformation reaches its maximum values at T_{ox} ~ 970 K. Comparison of the obtained results with the earlier data regarding PdO/SiO_2/Si (100) heterostructures synthesised in a dry oxygen atmosphere (with the partial pressure of oxygen of about 101.3 kPa) demonstrated that PdO films synthesized in an oxygen atmosphere are characterized by a higher degree of deformation of the crystal structure.

The effect of the oxidation temperature and O_2 partial pressure on the increase in the tetragonal lattice parameters of the PdO films can be explained by the formation of interstitial oxygen atoms in the octahedral void in the centre of the palladium(II) oxide unit cell.

Keywords: Palladium, Palladium(II) oxide, Heterostructures, Crystal structure, Gas sensors

Funding: The study was supported by the Ministry of Science and Higher Education of the Russian Federation within the framework of state order to higher education institutions in the sphere of scientific research for 2023-2025 (project No. FZGU-2023-0006).

Acknowledgements: Powder diffraction, transmission electron microscopy, and reflection high-energy electron diffraction studies were conducted using the equipment of the Centre for Collective Use of Scientific Equipment of VSU.

For citation: Samoylov A. M., Kopytin S. S., Ivkov S. A., Ratkov E. A., Tutov E. A. The effect of the synthesis conditions on the crystal structure of palladium(II) oxide nanofilms. *Condensed Matter and Interphases*. 2023;25(2): 225–236. https://doi.org/10.17308/kcmf.2023.25/11104

Для цитирования: Самойлов А. М., Копытин С. С., Ивков С. А., Ратьков Е. А., Тутов Е. А. Влияние условий синтеза на кристаллическую структуру нанопленок оксида палладия (II). *Конденсированные среды и межфазные границы*. 2023;25(2): 225–236. https://doi.org/10.17308/kcmf.2023.25/11104

✉ Alexander M. Samoilov, e-mail: samoylov@chem.vsu.ru

1. Introduction

Creating a global system for monitoring the quality of atmospheric air is one of the most urgent scientific and technical problems of the 21st century [1]. Currently, a number of devices and technologies are used to detect poisonous and explosive gases in air. They include resistive gas sensors based on wide-band metal oxide semiconductors, which are widely used due to their reliability and a relatively low production cost [1–3]. Such devices are necessary for the prevention of technological and household incidents with explosive gases, as well as for security systems in various industrial processes that use poisonous or flammable volatile substances [1–4]. For 50 years, the materials most often used in scientific studies and industrial production of resistive gas sensors have been metal oxide semiconductors with an electronic type of conductivity, specifically tin(IV) oxide SnO_2 [1–6]. Impressive success in the development of gas sensors based on SnO_2 can be explained by the results of studying the physico-chemical patterns that describe and predict the nature of the interaction of the active layer surface with the molecules of detected gases [3, 6, 7]. It was established that *n*-type wide-band semiconductors, particularly SnO_2, are characterised by a rather narrow homogeneity region [3, 4, 6, 7]. Various authors have proved the nature of point defects, mainly oxygen vacancies, which are responsible for nonstoichiometry and electronic type of conductivity of these compounds [3–7].

Despite the popularity of metal oxide semiconductors with an electronic type of conductivity for the production of gas sensors, materials for the so-called "perfect sensor" with optimal functional parameters have not yet been found [8, 9]. Over the past decade, there has been a considerable increase in the interest in the study of sensor properties of wide-band metal oxide semiconductors with the *p*-type surface and the composites based on them [10].

Recent studies have demonstrated that *p*-type nanostructures with various types of morphological organisation based on palladium(II) oxide are promising materials for the production of gas sensors that can detect even very small concentrations of toxic gases, including ozone and nitrogen oxides, in atmospheric air [11–23].

Prototypes of gas sensors based on nanocrystalline PdO films are characterised by a short recovery period and good reproducibility of the sensor signal when detecting ozone and nitrogen dioxide NO_2 in atmospheric air [17, 20–22]. There is also evidence that sensors based on PdO are highly sensitive to organic compound vapours, carbon monoxide, and hydrogen [24–25], which is of utmost importance for the creation of a strong hydrogen energetics system.

Earlier experiments demonstrated [11–25] that gas sensors based on palladium(II) oxide nanostructures are compatible with similar devices based on metal oxide materials with an electronic type of conductivity [20, 24–25]. However, unlike SnO_2, a large number of basic physico-chemical properties of palladium(II) oxide have not been thoroughly studied yet. For instance, there is no phase diagram of the palladium-oxygen system, and the nature of point defects responsible for the p-type of conductivity of PdO is still a matter of debate [11, 15, 17, 19, 20]. The lack of this information makes it impossible to establish the mechanisms of interaction of the detected gases with the surface of nanostructures of palladium(II) oxide and largely hinders the practical application of gas sensors based on them. A detailed study of the changes in the crystal structure of nanosized PdO films depending on the synthesis conditions will help to get closer to solving the problem of nonstoichiometry of palladium(II) oxide and the nature of point defects [19].

The purpose of our study was to analyse the crystal structure of nanosized Pd films on SiO_2/Si (100) substrates during oxidation in atmospheric air in the temperature range T_{ox} = 573–1148 K and then compare it to the results of earlier experiments involving oxidation of Pd/SiO_2/Si (100) heterostructures in a dry oxygen atmosphere [18–19].

2. Experimental

Nanocrystalline films of metallic palladium with a thickness of ~ 35 nm were synthesised using thermal sublimation of palladium foil with the concentration of the main component of 99.998 at.% in a high vacuum (residual pressure ~ 10^{-10} Pa) on SiO_2/Si(100) substrates which were not heated. Since the SiO_2/Si(100) substrates were

not heated, ultradispersed layers were formed with the size of Pd crystallites between 2 and 6 nm. Crystallites of this size ensure uniform oxidation and formation of PdO [17–20]. The sickness of the initial films of metallic palladium determined by studying the cleavages of the Pd/SiO_2/Si(100) heterostructure using scanning electron microscopy was ~ 35 nm (varied within the range of 32-38 nm).

The thickness of the SiO_2 buffer layer was about 300 nm. [18, 19] demonstrated that the SiO_2 buffer layer helps to prevent direct interaction between metallic palladium and the material of the substrate resulting in the formation of palladium silicide Pd_2Si. The oxidation of Pd films grown on Si(100) substrates without a SiO_2 buffer layer in an O_2 atmosphere in the temperature range T_{ox} = 970 – 1070 K resulted in the formation of palladium silicide Pd_2Si [18].

In our study, thermal oxidation of the formed ultradispersed Pd films was performed by heating in air. Pd/SiO_2/Si (100) heterostructures were put into a resistive heating tube furnace at room temperature and then heated to the set temperature at a rate of 250 degrees per hour. After reaching the set temperature, the heterostructures were exposed to isothermal endurance for 120 minutes.

When choosing the oxidation conditions for the ultradispersed Pd layers, we took into account the conditions under which the same process was conducted in an oxygen atmosphere [18, 19]. The oxidation conditions of the initial films of metallic Pd in air are given in Table 1.

Table 1 demonstrates that in some cases, specifically when the oxidation temperature was T_{ox} = 773 K and T_{ox} = 973 K, the duration of oxidation in air was 120 and 240 minutes. After the isothermal endurance, the samples were cooled together with the furnace.

The phase compositions and the crystal structures of the samples obtained by means of oxidation of the initial metallic Pd layers on SiO_2/Si (100) substrates were analysed using X-ray powder diffraction analysis (XRD) and reflection high-energy electron diffraction (RHEED). DRON-4-07 and Philips PANalytical X'Pert diffractometers with Cu$K\alpha$ or Co$K\alpha$ and an ER–100 electronograph were used. X-ray diffraction patterns of the samples were registered with rotation of the samples, while the profiles of X-ray reflections were constructed pointwise with the step of the counter being 0.01°. The most intense reflection (400) of the Si (100) substrate served as an internal standard to prevent accidental errors. Reflections of the Si (100) substrate and Pd and PdO films were identified using an international database [27–28].

Precise determination of the tetragonal crystal lattice period of palladium(II) oxide films was conducted by extrapolating the diffraction

Table 1. Synthesis conditions of nanocrystalline films of palladium(II) oxide by means of oxidation of ~ 35 nm ultradispersed films of metallic palladium in air and in an oxygen atmosphere [18, 19]

Temperature T_{ox}, K	Oxidation in oxygen atmosphere [18, 19]			Oxidation in atmosphere air (this work)		
	Duration τ, minutes	Phase composition of samples	Phase composition of samples	Duration τ, minutes	Phase composition of samples	Phase composition of samples
573	120	Heterogeneous	Pd + PdO	120	Homogeneous	Pd
623	120	Homogeneous	PdO	120	Heterogeneous	Pd + PdO
673	120	Homogeneous	PdO	120	Homogeneous	PdO
773	120	Homogeneous	PdO	120	Homogeneous	PdO
873	120	Homogeneous	PdO	120 и 240	Homogeneous	PdO
923	120	Homogeneous	PdO	120	Homogeneous	PdO
973	120	Homogeneous	PdO	120 и 240	Homogeneous	PdO
1023	120	Homogeneous	PdO	120	Homogeneous	PdO
1073	120	Homogeneous	PdO	120	Homogeneous	PdO
1098	120	Homogeneous	PdO	120	Heterogeneous	Pd + PdO
1123	120	Heterogeneous	PdO + Pd	120	Homogeneous	Pd
1148	120	Heterogeneous	Pd + PdO	120	Homogeneous	Pd

angle to θ = 90 degrees. For this, an extrapolation function $f(\theta)$ was chosen so that the dependence of parameters a and c on the value of $f(\theta)$ was closest to linear. The best results were obtained using the Nelson–Riley extrapolation function [27]:

$$f(\theta) = 0,5\left(\frac{\cos^2\theta}{\theta} + \frac{\cos^2\theta}{\sin\theta}\right), \quad (1)$$

where θ – is the diffraction angle.

The lattice constants a and c of the tetragonal structure of palladium(II) oxide were calculated using a software based on an algorithm for solving a system of quadratic equations with two non-obvious parameters, as well as the UnitCell software. We should note that the results calculated using two different methods correlate with each other within the experimental error. The values of the tetragonal lattice parameters were calculated by means of linear function approximation using the least squares method:

$$a = k \times f(\sin\theta) + a_0, \quad (2a)$$

$$c = k \times f(\sin\theta) + c_0. \quad (2b)$$

3. Results and discussion

Results of the XRD and RHEED analyses of the samples obtained by means of oxidation in air of ultradispersed layers of metallic Pd on SiO_2/Si (100) substrates in the temperature range T_{ox} = 573–1148 K are presented in Fig. 1 and 2 respectively. A characteristic RHEED pattern of single-phase nanocrystalline PdO films is given in Fig. 1. The XRD patterns of homogeneous Pd layers as well as heterogeneous samples (PdO + Pd) are given in Fig. 2 in the form of line diagrams of powder pattern. Since the reflections of nanocrystalline Pd and PdO films are 3–4 times less intense than the reflection of the Si (400) substrate, Fig. 2 shows the intensity of X-ray diffraction peaks on a logarithmic scale.

Comparison of the results of earlier experiments involving oxidation of Pd/SiO_2/Si (100) heterostructures in an oxygen atmosphere [18, 19] with the analysis of the phase state of the films obtained by means of oxidation of initial layers of metallic Pd in air is given in Table 1 and Fig. 3.

Fig. 2b and Table 1 demonstrate that the XRD analysis did not register any changes in the phase composition after the oxidation of the initial Pd films at T_{ox} = 573 K in atmospheric air. In other words, Pd is not oxidized in air at this temperature, as the PdO phase was not registered.

On the contrary, at the temperatures of T_{ox} = 873 K and T_{ox} = 973 K, the oxidation is fast and complete. When the duration of oxidation was two times longer, the diffraction patterns did not differ from those of the samples oxidised for 120 minutes. Therefore, we can say that 120 minutes is enough to reach the practical thermodynamic conditions required for oxidation.

Fig. 2c shows that after the oxidation in air at T_{ox} = 623 K, heterogeneous samples (Pd + PdO) are formed. The diffraction pattern registered Pd reflections and several most intense PdO reflections. The XRD and RHEED analyses demonstrated that single-phase PdO films are formed after the oxidation in air at T_{ox} = 673–1073 K (Table1, Fig. 3). When the oxidation temperature

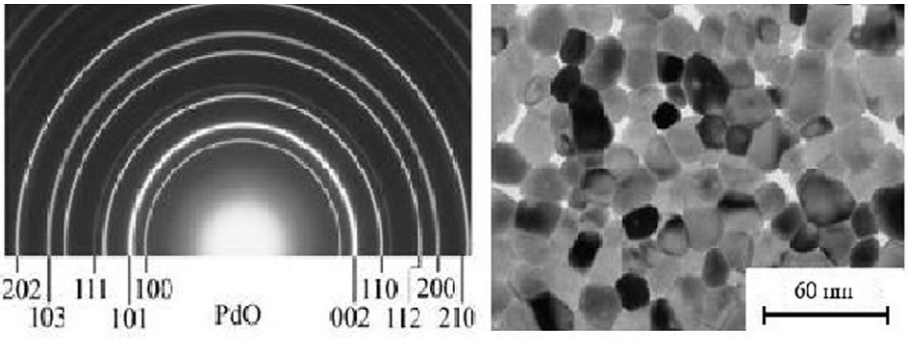

a b

Fig. 1. Reflection high-energy electron diffraction pattern (*a*) and a bright field TEM image (b) of single-phase (homogeneous) nanocrystalline PdO films obtained by oxidation of the initial ultradispersed palladium layers in atmospheric air at T_{ox} = 873 K

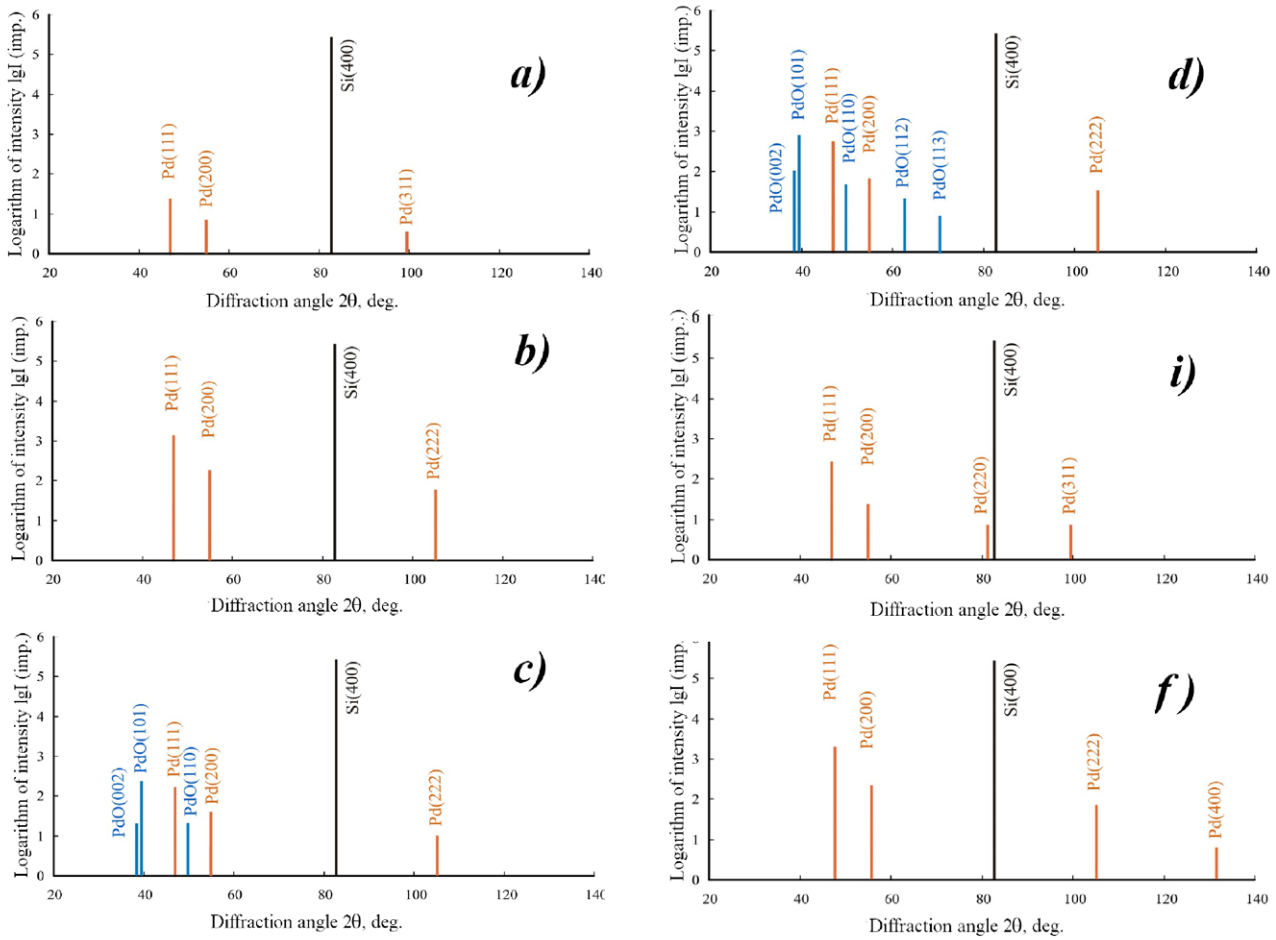

Fig. 2. X-ray diffraction patterns of samples synthesised by oxidation of ultradispersed films of metallic Pd on SiO_2/Si (100) substrates in atmospheric air in the temperature range T_{ox} = 573 – 1148 K: *a*) initial Pd/SiO_2/Si heterostructure; b) T_{ox} = 573 K; *c*) T_{ox} = 623 K; *d*) T_{ox} = 1098 K; *e*) T_{ox} = 1123 K; *f*) T_{ox} = 1148 K; Co*K*α-radiation

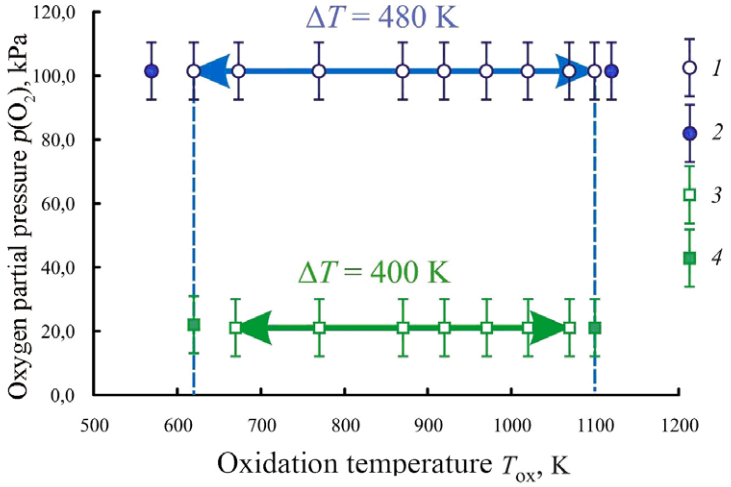

Fig. 3. XRD and RHEED patterns of films obtained by oxidation of the initial ultradispersed layers of metallic Pd on SiO_2/Si (100) substrates in air and in an oxygen atmosphere: *1*, *3* – single-phase PdO samples; *2*, *4* – heterogeneous samples PdO + Pd; *1*, *2* – oxidation in an oxygen atmosphere, data obtained in [18, 19]; *3*, *4* – oxidation in air, data obtained in the study

was raised to T_{ox} = 1098 K, heterogeneous samples were formed (Fig. 2d). The diffraction patterns of such samples registered PdO reflections and several metallic Pd reflections. Oxidation in air at T_{ox} > 1098 K results in the complete thermal decomposition of palladium(II) oxide films and the formation of metallic palladium (Fig. 2e and f).

Fig. 3 presents a comparison of the experimental results obtained in our study with the results presented in [18, 19] regarding the phase state of ultradispersed Pd films after oxidation in an oxygen atmosphere. The figure shows that the results obtained in this study are in qualitative agreement with the data presented in [18, 19]. There are only quantitative differences. For instance, homogeneous PdO films were formed after oxidation in an O_2 atmosphere [18, 19] at T_{ox} = 623 K, while during the oxidation in air homogeneous PdO samples were obtained only at T_{ox} = 673 K (Fig. 3). In our study, we also determined that thermal decomposition of homogeneous PdO layers in air followed by the formation of metallic Pd occurs at lower temperatures as compared to oxidation in oxygen. When oxidised in air, heterophase PdO + Pd layers were formed at T_{ox} = 1098 KK, while when oxidised in an oxygen atmosphere, thermal decomposition of homogeneous palladium(II) oxide films was only registered at T_{ox} = 1123 K (Fig. 3).

Therefore, we can say that replacing oxygen with atmospheric air for the oxidation process results in a significant reduction (by about 80 K) in the range of oxidation temperatures ensuring the formation of homogeneous PdO films. Taking into account the fact that Pd does not react with nitrogen in the studied temperature range [30], we can say that the oxidation process of Pd resulting in the formation of PdO is largely affected by the partial pressure of oxygen (Fig. 3).

Based on the diffraction patterns of the $Pd/SiO_2/Si$ (100) samples after thermal oxidation in air, we calculated the parameters of the tetragonal crystal lattice of palladium(II) oxide. The comparison of the calculations with the results obtained in [18, 19] is presented in Fig. 4.

Fig. 4 shows that nanocrystalline PdO films on $SiO_2/Si(100)$ substrates demonstrated non-monotonic change in the parameters of the tetragonal crystal lattice depending on the oxidation temperature. Non-monotonic change in parameters *a* and *c* of the tetragonal crystal lattice was registered for PdO films obtained by oxidation both in air and in an oxygen atmosphere (Fig. 4). When the oxidation temperature was increased to T_{ox} ~ 973 K, we observed a monotonous increase in parameters *a* and *c* of the tetragonal crystal lattice of single-phase PdO films regardless of the oxidation atmosphere. Further increase in the oxidation temperature at T_{ox} > 973 K was followed by a decrease in the *a* and *c* parameters of the tetragonal crystal lattice (Fig. 4). The sharpest decrease in the parameters *a* and *c* was registered at T_{ox} > 1073 K.

Despite the similarity of curves $a = f(T_{ox})$ and $c = f(T_{ox})$ of PdO films synthesised by means of oxidation of the initial ultradispersed palladium layers in air and in an oxygen atmosphere, there are some quantitative differences. Fig. 4 shows that in order to determine the differences we compared the results of this study and the ones obtained in [18, 19] with the latest data from an international crystallographic database [28]. The figure demonstrates that there are temperature ranges, in which parameters *a* and *c* of the tetragonal crystal lattice of nanosized PdO films are larger than those of the reference sample presented in the international crystallographic database [28].

Fig. 4a demonstrates that it is especially noticeable for the parameter *a* of the tetragonal crystal lattice of palladium(II) oxide films. At the same time, the range of such temperatures for the samples oxidised in an oxygen atmosphere (ΔT_{ox} = 773–1073 K) is significantly larger than that of the samples oxidised in air (ΔT_{ox} = 923–1073 K). We also calculated the absolute increase in the parameter Δa using the following formula:

$$\Delta a = a_{exp} - a_{ref}, \quad (3)$$

where a_{exp} is the experimental value; a_{ref} is the reference value of the ASTM sample.

For the films synthesised in oxygen, parameter Δa was almost three times larger than that of the samples oxidised in air.

Fig. 4b demonstrates that parameter *c* of the tetragonal crystal lattice of palladium(II) oxide films oxidised in air is lower than that of the ASTM standard sample [28]. At the same time, according to [18, 19], parameter *c* of the tetragonal crystal

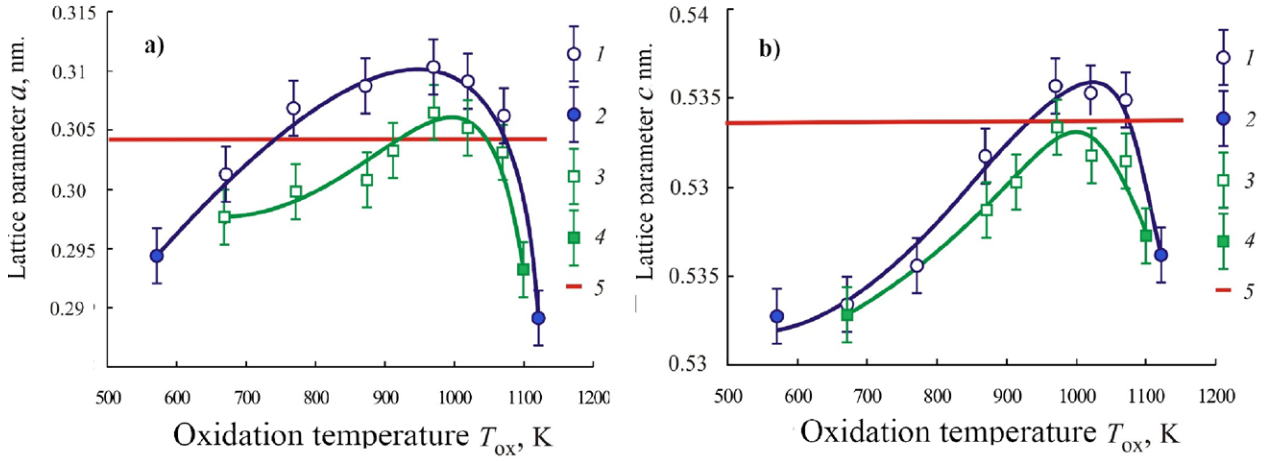

Fig. 4. Dependence of the *a* and *c* parameters of the tetragonal crystal lattice of nanosized PdO films synthesised by oxidation of the initial ultradispersed layers of metallic Pd on SiO_2/Si (100) substrates in air and in an oxygen atmosphere on the oxidation temperature T_{ox}: *1*, *3* – single-phase PdO samples; *2*, *4* – heterogeneous samples PdO + Pd; *1*, *2* – oxidation in an oxygen atmosphere, data obtained in [18, 19]; *3*, *4* – oxidation in air, data obtained in the study; *5* – ASTM reference sample [28]

lattice of palladium(II) oxide films oxidised in an O_2 atmosphere is higher than the ASTM standard parameter in the range of oxidation temperatures T_{ox} = 923–1073 K.

Therefore, we can say that the distortion of the tetragonal crystal lattice of palladium(II) oxide films obtained by oxidation in air, as compared to the ASTM standard [28], occurs mainly due to an increase in parameter *a* (Fig. 4a).

In this work, the values of the ratio of the *c*/*a* parameters were calculated for a more accurate estimate of the contribution of changes in the *a* and *c* parameters to the overall picture of deformation phenomena in the tetragonal lattice of nanocrystalline PdO films. It is known that the *c*/*a* ratio is a parametric feature of crystals of the middle category and it reflects the degree of anisotropy of the crystal structure and a number of physical properties.

The change in the *c*/*a* values for nanocrystalline PdO films depending on the oxidation temperature T_{ox} is presented in Fig. 5. As the figure shows, the *c*/*a* values for all single-phase nanocrystalline PdO films obtained by oxidation in oxygen in the temperature range of 600 K< T_{ox} <1050 K [18, 19] are significantly lower than the value calculated for the reference sample from the ASTM database [28]. On the contrary, the *c*/*a* values of heterogeneous samples (PdO + Pd) are higher than the similar value of the reference sample.

For the homogeneous PdO films obtained by oxidation in air, the *c*/*a* values are higher than the value calculated for the reference sample only in a limited temperature range of 923 K < T_{ox} < 1050 K (Fig. 5). When oxidised at low temperatures of 673 K < T_{ox} < 873 K in air, the *c*/*a* values were almost the same as the reference.

Curve $c/a = f(T_{ox})$ presented in Fig. 5 demonstrates a flat minimum in the temperature range 800 < T_{ox} < 850 K for PdO films obtained by oxidation in oxygen. For nanocrystalline PdO samples synthesised by oxidation in air, the minimum on curve $c/a = f(T_{ox})$ shifted to higher temperatures T_{ox} ~ 973 K (Fig. 5).

We should also note that nanosized PdO films obtained by oxidation in an O_2 atmosphere [18, 19] demonstrated greater deformation of the tetragonal lattice as compared to the reference sample in the ASTM database [28] than the samples obtained by oxidation in air (Fig. 5). This is reflected in the absolute values of the change in the parametric ratio $c/a = f(T_{ox})$ as well as in an increase in the range of oxidation temperatures in which the distortions were registered (Fig. 5).

The behaviour of the $c/a = f(T_{ox})$ curves of nanosized PdO films regardless of the synthesis conditions is another evidence proving that an increase in the parameters of the tetragonal lattice of nanocrystalline PdO films is not

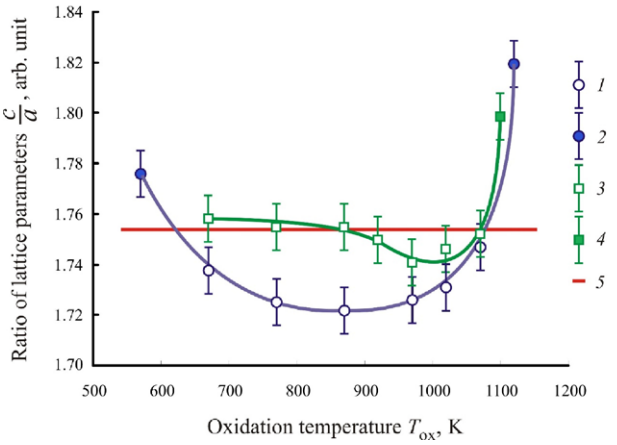

Fig. 5. Dependence of the *c*/*a* ratio of the tetragonal crystal lattice of nanosized PdO films synthesised by oxidation of the initial ultradispersed layers of metallic Pd on SiO_2/Si (100) substrates in air and in an oxygen atmosphere on the oxidation temperature T_{ox}: *1*, *3* – single-phase PdO samples; *2*, *4* – heterogeneous samples PdO + Pd; *1*, *2* – oxidation in an oxygen atmosphere, data obtained in [18, 19]; *3*, *4* – oxidation in air, data obtained in the study; *5* – ASTM reference sample [28]

uniform. The main contribution to the distortions of the tetragonal crystal structure of palladium(II) oxide occurs mainly due to an increase in the values of the *a* parameter, which is due to an increase in elementary translations along the *OX* and *OY* axes.

The above analysis of the transformations of the tetragonal structure of nanocrystalline PdO films depending on the oxidation temperature, demonstrated that the distortion is not uniform mainly due to an increase in the parameter *a*. This analysis needs to be complemented with the calculations of the unit cell volume of the crystal structure of palladium(II) oxide. Such calculations allow assessing the average degree of distortion of the tetragonal structure of nanocrystalline PdO films.

Based on the experimental data (Fig. 3), we calculated the unit cell volume V_{uc} of the tetragonal structure of nanocrystalline PdO films using the formula:

$$V_{uc} = a^2c, \quad (4)$$

where V_{uc} – is the unit cell volume; *a* and *c* – are parameters of the tetragonal crystal lattice of palladium(II) oxide.

The results of the calculations and their comparison with the data obtained in [18, 19] are given in Fig. 6 as a dependence $V_{uc} = f(T_{ox})$. As the figure shows, the unit cell volume V_{uc} of the crystal structure of single-phase nanocrystalline PdO films monotonously grows with an increase in the oxidation temperature from T_{ox} = 673 K to T_{ox} = 973 K regardless of the oxidation atmosphere. The maximum values of V_{uc} are found in the temperature range of 950 < T_{ox} < 980 K. At the same time, in the temperature range of T_{ox} = 773–1073 K the values of the unit cell volume V_{uc} for PdO films synthesised in oxygen atmosphere exceed the volume of the ASTM reference unit cell [28]. For PdO films obtained by oxidation in air, the range of temperatures in which V_{uc} exceeds the V_{uc} of the reference sample is far below T_{ox} = 873–1050 K.

The values of the X-ray density were calculated for a fuller picture of the analysis of the deformations in the structure of nanocrystalline PdO films. The X-ray density ρ_{Xray}(PdO) was calculated using the formula:

$$\rho_{Xray}(PdO) = \frac{2M(PdO)}{V_{uc} \cdot N_A}, \quad (5)$$

where *M*(PdO) – is the molar mass of palladium(II) oxide; V_{uc} – is the unit cell volume; N_A – is Avogadro number.

The results calculated using formula (5) for the samples obtained by oxidation in air are presented in Fig.7 as dependence $\rho_{Xray}(PdO) = f(T_{ox})$ in comparison with the data obtained earlier [18, 19]. The figure shows that the values of ρ_{Xray}(PdO) of PdO films synthesised by oxidation in both oxygen and air monotonously decrease with an increase in the oxidation temperature up to a minimum of T_{ox} ~ 970 K. We should note that the maximum values of density ρ_{Xray}(PdO) were obtained for heterogeneous samples (PdO + Pd) synthesised at T_{ox} = 573 K and T_{ox} = 1123 K respectively [18, 19].

Comparison of the calculated dependences $\rho_{Xray}(PdO) = f(T_{ox})$ with that of the ASTM reference sample (Fig. 7) demonstrated that homogeneous nanocrystalline PdO films obtained by oxidation in air in the temperature range of 970 < T_{ox} < 1050 are characterised by densities lower than those of the reference sample [28]. Minimum values of the X-ray density of PdO samples synthesised

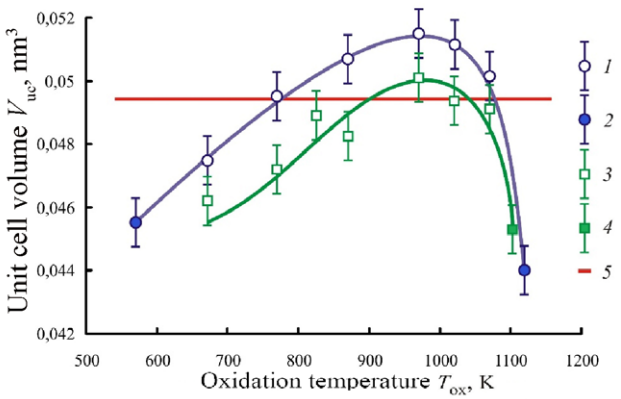

Fig. 6. Dependence of the unit cell volume V_{uc} of the tetragonal crystal lattice of nanocrystalline PdO films synthesised by oxidation of the initial ultradispersed layers of metallic Pd on SiO_2/Si (100) substrates in air and in an oxygen atmosphere on the oxidation temperature T_{ox}: *1*, *3* – single-phase polycrystalline PdO samples; *2*, *4* – heterogeneous samples (PdO + Pd); *1*, *2* – oxidation in an oxygen atmosphere, data obtained in [18, 19]; *3*, *4* – oxidation in air, data obtained in the study; *5* – ASTM reference sample [28]

in an O_2 atmosphere were registered in a much larger temperature range of 770 < T_{ox} < 1070 K. Nanocrystalline PdO films synthesised at lower temperatures (570 < T_{ox} < 770), as well as at T_{ox} > 1070 K are characterised by a higher X-ray density as compared to the ASTM reference sample [28].

Fig. 7 also shows the density of polycrystalline ρ(PdO) powders of palladium(II) oxide determined by means of hydroscopic weighing [30]. The figure demonstrates that the ρ_{Xray}(PdO) of the ASTM reference sample and ρ(PdO) determined by means of hydroscopic weighing are close to each other.

When analysing the nature of deformations of homogeneous nanocrystalline PdO films (Fig. 4–7), we should point out that the degree of distortion of the crystal lattice of homogeneous nanocrystalline PdO films depends more on the oxidation atmosphere rather than the temperature. The maximum deformation of the tetragonal lattice was observed in PdO films obtained by oxidation in oxygen with the value of partial pressure $p(O_2)$ ~101–103 kPa (Fig. 3).

When discussing the obtained results, it is necessary to take into account the fact that PdO samples are characterised by p-type conductivity [12, 15, 17], which, from the point of view of solid state chemistry, is explained by the presence of negatively charged interstitial atoms of oxygen. Incorporation of excess oxygen atoms (with regard to the stoichiometric ratio of PdO) confirms a decrease in the density caused by an increase in the portion of a lighter component - oxygen. Therefore, taking into account the unit cell model of palladium(II) oxide suggested in [18], possible ways of incorporation of oxygen atoms into the crystal lattice of palladium(II) oxide are given in Fig 8.

It is also known [30] that palladium can form compounds with the oxidation state (+4). Palladium(IV) oxide is characterised by a crystal structure of the rutile type TiO_2. The palladium-oxygen coordination number is 6, and the coordination polyhedron is an octahedron. Therefore, oxygen atoms can be incorporated between neighbouring palladium atoms in the crystal structure of palladium(II) oxide as shown in Fig. 8.

Taking into account the unit cell model of palladium(II) oxide [18], interstitial oxygen atoms should be located in the octahedral void in the centre of the cell with coordinates $\left[\left[\frac{1}{2}\frac{1}{2}\frac{1}{2}\right]\right]$.

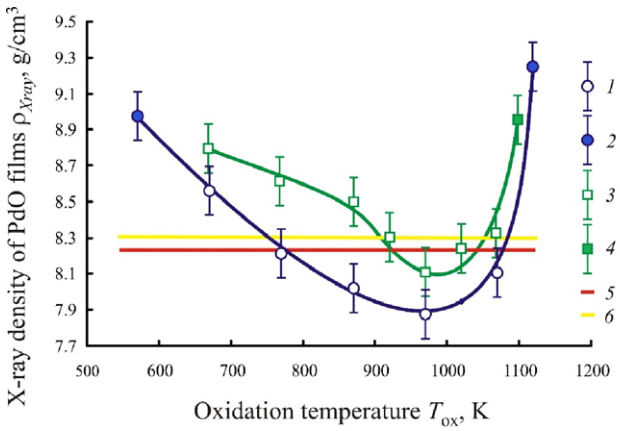

Fig. 7. Dependence of the X-ray density of nanocrystalline PdO films synthesised by oxidation of the initial ultradispersed layers of metallic Pd on SiO2/Si (100) substrates in air and in an oxygen atmosphere on the oxidation temperature T_{ox}: *1*, *3* – single-phase polycrystalline PdO samples; *2*, *4* – heterogeneous samples (PdO + Pd); *1*, *2* – oxidation in an oxygen atmosphere, data obtained in [18, 19]; *3*, *4* – oxidation in air, data obtained in the study; *5* – ASTM reference sample [28]; *6* – data obtained by means of hydrostatic weighing [30]

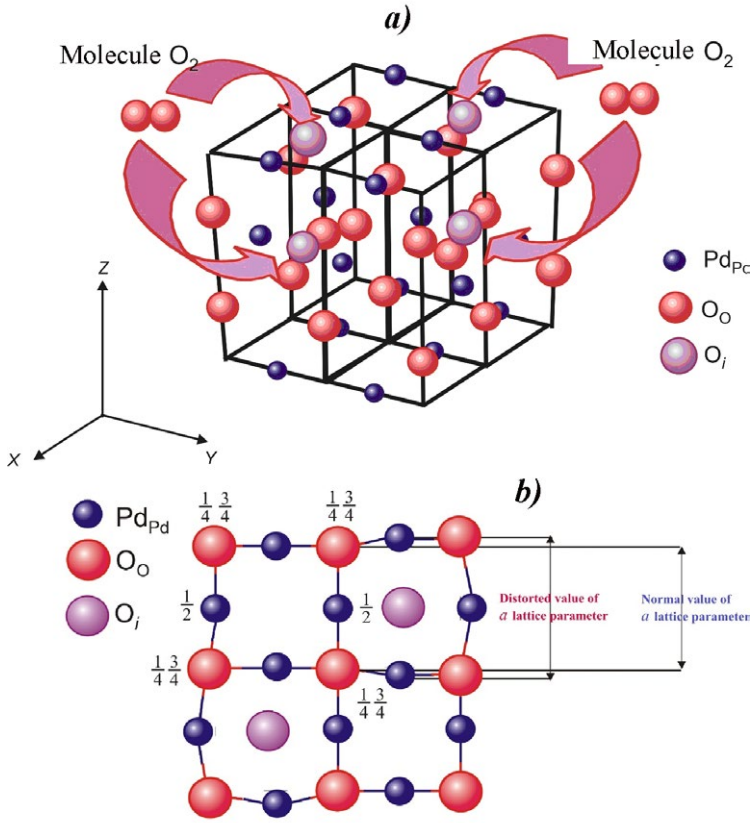

Fig. 8. A scheme explaining the deformations in the tetragonal crystal structure of nanocrystalline PdO films by the incorporation of interstitial oxygen atoms: *a*) a spatial 3D model of four unit cells of the crystal lattice of palladium(II) oxide; b) a projection of four unit cells of PdO on the plane *XOY*

4. Conclusions

1. The XRD and RHEED analyses determined that the oxidation of the initial ultradispersed layers of metallic palladium in air results in the formation of homogeneous polycrystalline films of palladium(II) oxide on SiO_2/Si (100) substrates in the temperature range T_{ox} = 673–1073 K. The temperature range is significantly wider, when the oxidation is conducted in an oxygen atmosphere.

2. Based on the calculation of the changes in the parameter ratio of the tetragonal lattice of nanocrystalline PdO films, we demonstrated that the distortions of the crystal lattice are mainly due to an increase in the value of parameter *a*.

3. The study demonstrated that the degree of distortion of the crystal lattice of homogeneous nanocrystalline PdO films depends on the oxidation atmosphere rather than on the temperature. The maximum deformation of the tetragonal lattice was observed in PdO films obtained by oxidation in oxygen with the value of partial pressure $p(O_2)$ ~101–103 kPa.

4. The article suggested a model which explains the distortions in the tetragonal lattice of nanocrystalline films of palladium(II) oxide by the incorporation of excess oxygen atoms into interstitial sites of the unit cell, preferably into the octahedral void in the centre of the cell with coordinates $\left[\left[\frac{1}{2}\frac{1}{2}\frac{1}{2}\right]\right]$.

Contribution of the authors

The authors contributed equally to this article.

Conflict of interests

The authors declare that they have no known competing financial interests or personal relationships that could have influenced the work reported in this paper.

References

1. Yamazoe N. Toward innovations of gas sensor technology. *Sensors and Actuators B*. 2005;108: 2–14. https://doi.org/10.1016/j.snb.2004.12.075

2. Seiyama T., Kato A., Fujiishi K., Nagatani M. A new detector for gaseous components using semiconductive thin tilms. *Analytical Chemistry*. 1962;34: 1502–1503. https://doi.org/10.1021/ac60191a001

3. Marikutsa A. V., Rumyantseva M. N., Gaskov A. M., Samoylov A. M. Nanocrystalline tin dioxide: Basics in relation with gas sensing phenomena. Part I. Physical and chemical properties and sensor signal formation. *Inorganic Materials*. 2015;51(13): 1329–1347. https://doi.org/10.1134/S002016851513004X

4. Ong C. B., Ng L. Y., Mohammad A. W. A review of ZnO nanoparticles as solar photocatalysts: synthesis, mechanisms and applications. *Renewable and Sustainable Energy Reviews*. 2018;81: 536–551. https://doi.org/10.1016/j.rser.2017.08.020

5. Korotcenkov G. Metal oxides for solid-state gas sensors: What determines our choice? *Materials Science and Engineering: B*. 2007; 139: 1–23. https://doi.org/10.1016/j.mseb.2007.01.044

6. Marikutsa A. V., Rumyantseva M. N., Gaskov A. M., Samoylov A. M Nanocrystalline tin dioxide: Basics in relation with gas sensing phenomena. Part II. Active centers and sensor behavior. *Inorganic Materials*. 2016;52(13): 1311–1338. https://doi.org/10.1134/S0020168516130045

7. Al-Hashem M., Akbar S., Morris P. Role of oxygen vacancies in nanostructured metal-oxide gas sensors: a review. *Sensors Actuators B*. 2019;301: 126845. https://doi.org/10.1016/j.snb.2019.126845

8. Korotcenkov G. *Handbook of gas sensor materials. Properties, advantages and shortcomings for applications. Volume 1: Conventional approaches*. Springer: New York Heidelberg Dordrecht London; 2013. 442 p. https://doi.org/10.1007/978-1-4614-7165-3

9. Toda K., Furue R., Hayami S. Recent progress in applications of graphene oxide for gas sensing: A review. *Analytica Chimica Acta*. 2015;878: 43–53. https://doi.org/10.1016/j.aca.2015.02.002

10. Kim H.-J., Lee J.-H. Highly sensitive and selective gas sensors using *p*-type oxide semiconductors: Overview. *Sensors and Actuators B*. 2014;192: 607–627. https://doi.org/10.1016/j.snb.2013.11.005

11. García-Serrano O., López-Rodríguez C., Andraca-Adame J. A., Romero-Paredes G., Pena-Sierra R. Growth and characterization of PdO films obtained by thermal oxidation of nanometric Pd films by electroless deposition technique. *Materials Science and Engineering B*. 2010;174: 273–278. https://doi.org/10.1016/j.mseb.2010.03.064

12. Ryabtsev S. V., Ievlev V. M., Samoylov A. M., Kuschev S. B., Soldatenko S. A. Microstructure and electrical properties of palladium oxide thin films for oxidizing gases detection. *Thin Solid Films*. 2017;636: 751–759. https://doi.org/10.1016/j.tsf.2017.04.009

13. Ryabtsev S. V., Shaposhnik A. V., Samoylov A. M., Sinelnikov A. A., Soldatenko S. A., Kuschev S. B., Ievlev V. M. Thin films of palladium oxide for gas sensors. *Doklady Physical Chemistry*. 2016;470(2): 158–161. https://doi.org/10.1134/s0012501616100055

14. Ryabtsev S. V., Iyevlev V. M., Samoylov A. M., Kuschev S. B., Soldatenko S. A. Real microstructure and electrical properties of palladium oxide thin films for oxidizing gases detecting. In: *Science and Application of Thin Films, Conference & Exhibition (SATF-2016)* Çeşme*, Izmir, Turkey, September 19–23, 2016. Book of Abstracts: Izmir Institute of Technology*. 2016: 44.

15. Ievlev V. M., Ryabtsev S. V., Shaposhnik A. V., Samoylov A. M., Kuschev S. B., Sinelnikov A. A. Ultrathin films of palladium oxide for oxidizing gases detecting. *Procedia Engineering*. 2016;168: 1106–1109. https://doi.org/10.1016/j.proeng.2016.11.357

16. Samoylov A. M., Gvarishvili L. J., Ivkov S. A., Pelipenko D. I., Badica P. Two-stage synthesis of pPalladium (II) oxide nanocrystalline powders for gas sensor application. *Research & Development in Material Science*. 2018;8(2). https://doi.org/10.31031/rdms.2018.08.000682

17. Ievlev V. M., Ryabtsev S. V., Samoylov A. M., Shaposhnik A. V., Kuschev S. B., Sinelnikov A. A. Thin and ultrathin of palladium oxide for oxidizing gases detection. *Sensors and Actuators B*. 2018;255(2): 1335–1342. https://doi.org/10.1016/j.snb.2017.08.121

18. Samoylov A. M., Ivkov S. A., Pelipenko D. I., ... Badica P. Structural changes in palladium nanofilms during thermal oxidation. *Inorganic Materials*. 2020;56(10): 1020–1026. https://doi.org/10.1134/s0020168520100131

19. Samoylov A. M., Pelipenko D. I., Kuralenko N. S. Calculation of the nonstoichiometry area of nanocrystalline palladium (II) oxide films. *Condensed Matter and Interphases*. 2021;23(1): 62–72. https://doi.org/10.17308/kcmf.2021.23/3305

20. Samoylov A. M., Ryabtsev S. V., Popov V. N., Badica P. Palladium (II) oxide nanostructures as promising materials for gas sensors. In: *Novel nanomaterials synthesis and applications*. (George Kyzas ed.). UK, London: IntechOpen Publishing House; 2018. p. 211–229. https://doi.org/10.5772/intechopen.72323

21. Ryabtsev S. V., Ghareeb D. A. A., Sinelnikov A. A., Turishchev S. Yu., Obvintseva L. A., Shaposhnik A. V. Ozone detection by means of semiconductor gas sensors based on palladium (II) oxide. *Condensed Matter and Interphases*. 2021;23(1): 56–61. https://doi.org/10.17308/kcmf.2021.23/3303

22. Ryabtsev S. V., Ghareeb D. A. A., Turishchev S. Yu., Obvintseva L. A., Shaposhnik A. V., Domashevskaya E. P. Structural and gas-sensitive characteristics of thin semiconductor PdO films of various thicknesses during ozone detection. *Semiconductors*. 2022;56(13): 2057–2062. https://doi.org/10.21883/SC.2022.13.53898.9684

23. Samoylov A. M., Pelipenko D. I., Ivkov S. A., Tyulyakova E. S., Agapov B. L. Thermal stability limit of thin palladium(II) oxide films. *Inorganic Materials*. 2022;58(1): 48–55. https://doi.org/10.1134/s0020168522010095

24. Choudhury S., Bettya C. A., Bhattacharyyaa K., Saxenab V., Bhattacharya D. Nanostructured PdO thin film from Langmuir–Blodgett precursor for room temperature H_2 gas sensing. *ACS Applied Materials & Interfaces*. 2016;8(26): 16997–17003. https://doi.org/10.1021/acsami.6b04120

25. Yang S., Li Q., Li C., ... Fu Y. Enhancing the hydrogen-sensing performance of p-type PdO by modulating the conduction model. *ACS Appl. Mater. Interfaces*. 2021;13: 52754–52764. https://doi.org/10.1021/acsami.1c13034

26. *Phase diagrams of binary metal systems: Handbook: in 3 volumes**. Lyakishev N. P. (ed.) Moscow: Metallurgy Publ.; 1996–2000. (In Russ.)

27. Hammond C. *The basics of crystallography and diffraction*. Fourth edition. International union of crystallography. Oxford University Press; 2015. 519 p.

28. *ASTM JCPDS - International Centre for Diffraction Data*. ã 1987-2009. JCPDS-ICDD. Newtown Square, PA 19073. USA.

29. Grier D., McCarthy G., North Dakota: State University, Fargo, N. Dakota, USA, ICDD Grant-in-Aid, JCPDS-ICDD, 1991. Card no. 43-1024.

30. Wiberg, E., Wiberg, N., Holleman, A. F. *Inorganic Chemistry*. 1st English Edition. San Diego: Academic Press; Berlin, New York: De Gruyter, USA; 2001. 1884 p.

* *Translated by author of the article.*

Information about the authors

Alexander M. Samoilov, Dr. Sci. (Chem.), Associate Professor, Professor at the Department of Materials Science and Industry of Nanosystems, Voronezh State University (Voronezh, Russian Federation).

https://orcid.org/0000-0003-4224-2203

samoylov@chem.vsu.ru

Stanislav S. Kopytin, postgraduate student, Department of Materials Science and Industry of Nanosystems, Voronezh State University (Voronezh, Russian Federation).

https://orcid.org/0000-0001-9353-0219

kopytin-stanislav@rambler.ru

Sergey A. Ivkov, PhD (Phys.-Math.), Leading Electronics Engineer, Department of Solid State Physics and Nanostructures, Voronezh State University (Voronezh, Russian Federation).

https://orcid.org/0000-0003-1658-5579

ivkov@phys.vsu.ru

Egor A. Ratkov, master degree student, Voronezh State University (Voronezh, Russian Federation).

https://orcid.org/0009-0005-6848-1773

ratkov1511@gmail.com

Evgeny A. Tutov, Dr. Sci. (Chem.), Associate Professor, Department of Physics, Voronezh State Technical University (Voronezh, Russian Federation).

https://orcid.org/0000-0002-5481-8137

tutov_ea@mail.ru

Received 12.12.2022; approved after reviewing 10.01.2023; accepted for publication 15.02.2023; published online 25.06.2023

Translated by Yulia Dymant

Edited and proofread by Simon Cox